Noise Analysis in the Majorana Dark Matter Detector

Greg Dooley

INT REU at the University of Washington
Advisor: Mike Miller

August 28, 2010

Abstract

The Majorana Experiment seeks to detect neutrinoless double beta decay of ^{76}Ge with an array of customized ultra pure germanium detectors. It will simultaneously operate in a search for dark matter through direct detection of nuclear recoils with particles in a DM halo. Its ultimate DM goal is to probe down to energies of <1 KeV in a 120 kg Ge detector. Rather than distinguish between nuclear and electron recoil events, the detector will achieve such high sensitivity through extreme reduction of noise and background. A framework for minimizing electronic noise with a trapezoidal filter is established in this paper. The technique was applied to real data from the CoGeNT germanium crystal detector and an optimal peaking time parameter was found to be between .1 μS and 1 μS. Decomposition of the noise into parallel, series and 1/f components may suggest that the noise is dominated by parallel and series noise, but the results are inconclusive until further study is conducted.

1 Introduction

The Majorana project will search for neutrinoless double beta decays which would demonstrate that the neutrino is its own antiparticle: a majorana particle. Its semi-conductor detector will consist of ultra pure ^{76}Ge and intends to operate with extremely low background. It will be surrounded by pre WWII lead and placed several thousand feet underground in the Sanford Underground Laboratory in South Dakota for radiation shielding [1]. This makes it simultaneously very suitable as a dark matter detector, which is the focus of this project. In particular, the detector relies on dark matter to interact via the weak force in order to have a non-zero nuclear recoil cross section. It aims to detect WIMPs, Weakly Interacting Massive Particles, in a dark matter halo which Earth is passing through. The next stage in the project, the Majorana Demonstrator, aims to detect WIMPs in the $1 - 10$ GeV/c^2 range, and resolve energies of < 1KeV. This paper will explore how to minimize electronic noise in an effort to help achieve these goals.

2 Signal Processing

A positive dark matter detection would consist of a WIMP recoiling off a germanium nucleus within the detector. This process kicks electrons into the conduction band of the semi-conductor with the number of electrons released varying linearly with incident energy. The electrons are then accelerated to their maximal drift velocity by a large reverse biased electric field and accumulate on a capacitor. Electronics read the amount of charge on the capacitor over time, so a sudden increase in charge corresponds to some radiation detection. Fig 1 gives an example pulse of radiation detection. The rise time of the signal is limited by the drift velocity of electrons in the detector, which is very high for germanium as compared to other options. The height of the pulse corresponds to the energy of the collision. See [2] for more details on semi-conductor detectors.
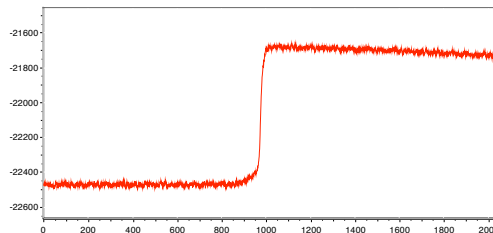

Figure 1: Electronic pulse from a radiation detection.

2.1 Trapezoidal Filter

Once a physics pulse is obtained, a trapezoidal filter is run over the data digitally to measure the pulse height and average out noise. This filter consists of two summation windows, each of length P, separated by a gap of length G. The filter runs across the voltage vs time data, summing values that coincide with the first window, and subtracting values that coincide with the second window. If we denote the input pulse as F, the filtered pulse as T and their value at each discrete time bin by the subscript i, then the filter computes the following [3]:

$$T_i = \sum_{k=0}^{P} F_{i-k} - \sum_{k=P+G}^{2P+G} F_{i-k} \qquad (1)$$

When applied to a pulse, the resultant shape is a trapezoid which peaks after a time $P + R$, has a flat top of width $G - R$, and falls back to 0 again in time $P + R$ where R is the rise time of the pulse. Thus P is called the peaking time, and G the gap time. The rise time is controlled by the detector and must be less than the gap time, or else the full pulse height will not be measured. This analysis assumes the gap time will be set in relation to the rise time and treats it as a constant parameter. An example trapezoid is shown in Fig 2.
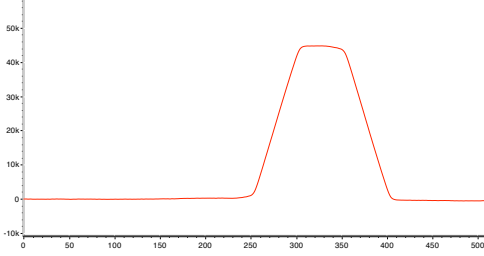

Figure 2: Signal produced after a trapezoidal filter runs over a pulse. The shape is described by a peaking time, P, and a gap time G which corresponds to the flat top width assuming negligible pulse rise time

3 Noise Analysis

The height of the trapezoid can be obscured by electronic noise in the system. When plotting an energy histogram, this contributes to the width of a mono energetic source's peak. We would like to be able to quantify, in terms of the peak's full width at half maximum, FWHM, what the contribution of electronic noise is for a given peaking time P. The procedure for finding this starts with the power spectrum of the electronic noise, $N(f)$ in units of $ADC/\sqrt{Hz}$. ADC is an arbitrary unit linearly proportional to the voltage of the noise and the amount of charge collected in the detector to produce an equivalent signal. This is multiplied by the transfer function for the trapezoidal filter, $H(f)$ to measure noise power after filtering. The resultant spectrum is then squared and integrated over all frequencies to obtain total RMS noise power in units of ADC^2. Taking the square root then multiplying by 2.35 and a calibration constant, C, gives the FWHM in units of energy. C is measured experimentally as the energy of a pulse in eV divided by its height in units of ADC. Symbolically:

$$FWHM(P) = 2.35C\sqrt{\int_0^\infty N(f)^2 \cdot H(f,P)^2 \, df} \quad (2)$$

Minimization of $FWHM(P)$ yields the optimal peaking time.

3.1 Components of Noise

The electronic noise power spectrum is measured experimentally, but it is useful to have an analytic description. Simplifying the electronics that read the capacitor in a model shown in Fig 3, there are three types of resultant noise: parallel, series, and 1/f. Parallel noise comes from shot noise and thermal (Johnson) noise in the detector capacitance and parallel resistance. Thermal noise in the series resistor makes up series noise, and 1/f noise is not well understood, but its power exhibits an inverse frequency dependence.

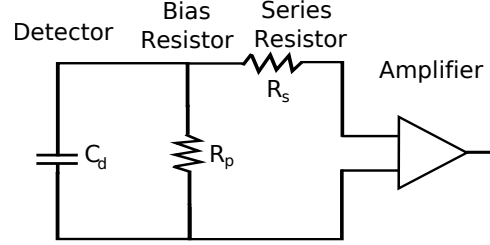
Figure 3: Simplified circuit

As derived in Spieler [4], these contributions are:

$$Parallel: V_p^2(f) = \frac{2q_e I_D}{(2\pi f C_D)^2} + \frac{4kTR_p}{1 + (2\pi f R_p C_D)^2} \quad (3)$$

$$Series: V_s^2(f) = 4kTR_s \quad (4)$$

$$1/f: V_o^2(f) = w/f \quad (5)$$

where q_e is the electron charge, I_D the detector current, k is Boltzmann's constant, T the temperature, and w is a constant. Defining the constants k_1, k_2, k_3, v, w necessary for Eqts 6, 7, 8, we can work with simplified forms since these constants cannot be deduced further with the method used.

$$Parallel: V_p^2(f) = \frac{k_1}{f^2} + \frac{k_2}{1 + k_3 f^2} \quad (6)$$

$$Series: V_s^2(f) = v \quad (7)$$

$$1/f: V_o^2(f) = w/f \quad (8)$$

3.2 Transfer Function

Now that the form of $N(f)$ has been found, the transfer $H(f)$ must be computed. Given an input signal $f(t)$, the trapezoidal function T acts on it to produce $O(t)$. $T(f(t)) = O(t)$ can be equivalently written as a convolution of f(t) with the impulse response of T, I(T):

$$f(t) \star I(t) = O(t). \quad (9)$$

Using the convolution theorem,

$$\mathcal{F}(f(t)) \cdot \mathcal{F}(I(t)) = \mathcal{F}(O(t)). \quad (10)$$

But $\mathcal{F}(f(t))$ is the initial power spectrum, and $\mathcal{F}(O(t))$ is the power spectrum after filtering, so $\mathcal{F}(I(t)) = H(f)$ as

desired. $I(t)$ is found by applying the filter to a function $i(t) = 1$ for $t = 0$ and $i(t) = 0$ everywhere else and is shown in Fig 4.
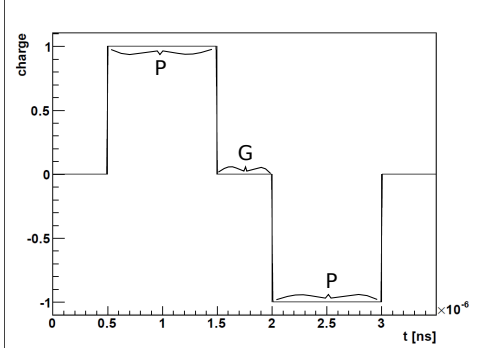

Figure 4: Impulse function for the trapezoidal filter.

Direct computation of the Fourier transform of a top hat of unit height and width P gives $\frac{sin(\pi f P)}{\pi f}$. Applying the linearity and translation properties of the transform to a top hat,

$$\mathcal{F}(I(t)) = e^{-2\pi i f(P+\frac{G}{2})}\frac{2i}{\pi f}sin(\pi f P)sin(\pi f(P+G)) \tag{11}$$

The imaginary components ordinarily matter in the function, but since the real and imaginary Fourier components of $\mathcal{F}(f(t))$ are independent random variables as shown in Figs 5 and 7, we can accurately use the magnitude of Eq 11. A critical addition to this method is in normalization of the power. Since a larger value of P corresponds linearly to a greater trapezoidal height for a given energy pulse, it will also nonphysically increase the magnitude of noise power after filtering with the current $H(f)$. Normalization requires division by P. Therefore,

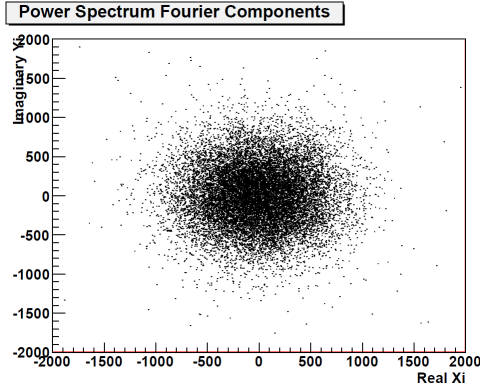$$H(f) = \frac{2}{\pi f P}sin(\pi f P)sin(\pi f(P+G)). \tag{12}$$

Figure 5: Fourier components of the noise power spectrum are randomly distributed.

An example transfer function for $P = 1 \times 10^{-6}s$ and $G = 5 \times 10^{-9}s$ is shown in Fig 6.
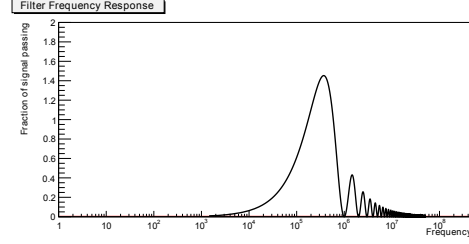

Figure 6: Trapezoidal filter transfer function for $P = 1 \times 10^{-6}s$ and $G = 5 \times 10^{-9}s$

3.3 FWHM^2 vs Peaking time

Plugging Eqs 6, 7, 8 and 12 into 2 and squaring the value, we can compute $FWHM(P)^2$. Defining $u = k_1 + \frac{k_2}{k_3}$ the result is of the form

$$FWHM(P)^2 = aP + b/P + c \tag{13}$$

where

$$a = const_P \times u^2 \tag{14}$$
$$b = const_S \times v^2 \tag{15}$$
$$c = const_F \times w^2. \tag{16}$$

Mathematica was unable to compute the constants analytically, but a python script reveals this proportionality is true when the integral is carried out to a large, but finite, frequency. The constants are computed with the script.

3.4 Simulated Noise

An additional objective of the noise analysis is to produce simulations. Following the method proven in [5], we define the mean of the power spectrum at a given frequency as μ. If the phase of the Fourier amplitude components, $tan^{-1}(Y_i/X_i)$, are uniformly distributed and X_i, Y_i are Gaussian distributed around 0 with standard deviation σ, then

$$\mu = 2\sigma^2. \tag{17}$$

Sampling μ from the power spectrum, the corresponding σ is used in generating random Fourier components. These are then inverse Fourier transformed into simulated noise. Demonstration of the necessary phase distribution is given in Fig 7 and the Gaussian distribution in Fig 8.

Application of this method produces realistic looking pulses. Fig 9 shows a simulated pulse, and Fig 10 shows a real pulse for comparison.

4 Analysis of Real Noise and Results

Using the CoGeNT detector, 6000 randomly triggered pulses were taken in order to sample the electronic noise.
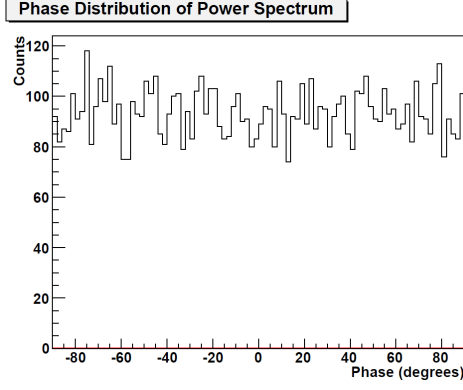
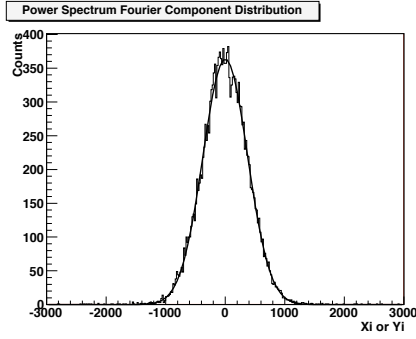Figure 7: The phase of the noise power spectrum is uniformly distributed.

Figure 8: The Fourier components of the noise power spectrum are Gaussian distributed. Smooth line is a Gaussian fit.
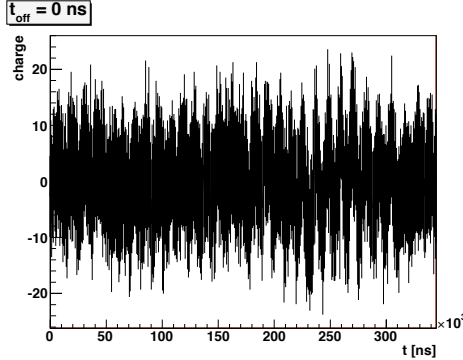

Figure 9: Simulated electronic noise

Each pulse was taken for 344.6 μS. The maximum frequency resolvable is set by $1/2 \times$ sampling rate = 50 MHz. The minimum frequency resolvable is 1/pulse duration = 2902 Hz. In order to eliminate pulses with physics signals and pulse resets, a simple veto was made to all waveforms not constrained to ± 30. A visual inspection suggests that this is an effective method, however a more precise way should be used to eliminate very
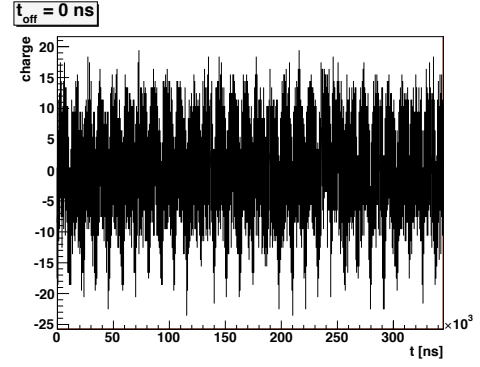

Figure 10: Real electronic noise

small signals if they exist. All pulses are transformed using MGDO [6] which uses FFTw3. The averaged power spectrum is given in Fig 11. The spectrum has many sig-
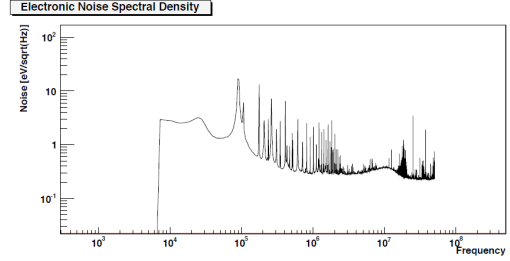

Figure 11: Electronic noise power spectrum calibrated to eV/$\sqrt{(Hz)}$

nificant features, in particular a spike at $80 kHz$. Their sources are not yet known and diagnostics still need to be performed to obtain a better signal. This spectrum is multiplied by filters of various peaking times and integrated to obtain the $FWHM(P)^2$ shown in Fig 12. Equation 13 is fitted to the curve and the values of a, b and c are given with errors. Changes in the array of peaking times used affects the parallel and series fit components little, but can have dramatic effects on the 1/f fit. This value should therefore not be interpreted as an accurate model of the electronic noise. A cleaner power spectrum may improve this.

Knowing the values of a, b and c, and computing the constants in Eqs 14, 15, 16, we find the corresponding values of u, v, and w. v and w are used to find the series and 1/f power spectrum components directly, but k_1, k_2, and k_3 cannot be deduced from u. Instead, a boundary condition is imposed matching the experimental spectrum to the sum of the extracted noise components. This obtains one additional constant. The analysis was done before realizing the need for k_1 and is thus only accurate if k_1 is small. More exploration needs to be done on finding the parallel component accurately. The attempt to reproduce the components in a power spectrum is shown
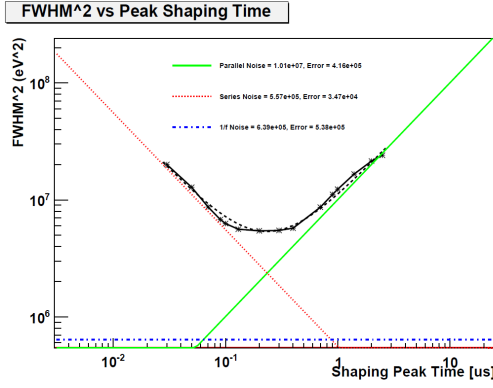
Figure 12: $FWHM^2$ as a function of peaking time. An optimal peaking time would be $.25\mu S$

in Fig 13. With large uncertainty in the 1/f noise, and an incomplete parallel noise fit, little can be deduced yet from the plot. However, the sum of components resemblance to the experimental data demonstrates that the approach is reasonable.
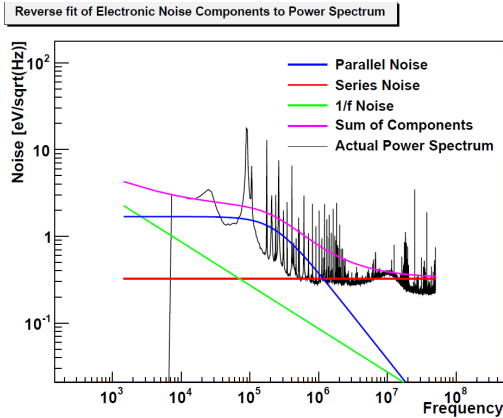

Figure 13: Plot of extracted noise components.

Attempts to fit the types of noise directly to the power spectra do not produce reliable results. In addition, a repeat analysis was made on a power spectrum that follows the experimental data except with all peaks removed by hand. This resulted in a $FWHM(P)^2$ curve that fits the ideal shape better and an optimal peaking time of around .8 μS, which is closer to the optimal time used in previous experiments. When ignoring the highly variable 1/f extraction, the parallel and series spectral density components sum close to the experimental curve. Direct fitting reinforces this as it obtains a decent fit with negligible 1/f contribution. While nothing quantitative can be reported yet, it is promising that a better electronic noise signal could yield informative results about its parallel and series composition.

4.1 Direct FWHM measurement

The electronic noise FWHM can also be directly measured by using a pulser to deposit charge in the detector capacitor. Using a peak from an actual radiation source will not work since incomplete charge collection and statistical fluctuation in the leakage current and charge generated also contribute to the width. This method was explored to verify features of the previous method. While results for five peaking times are plotted in Fig 14, they should not be trusted until more work is done. Using
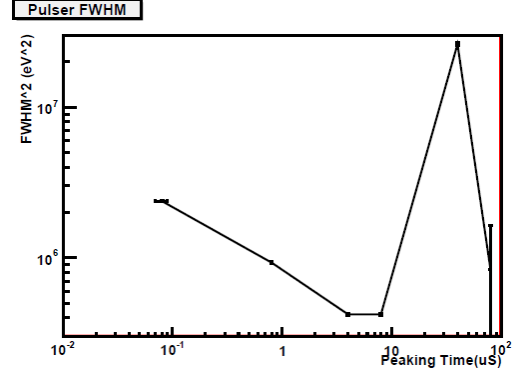

Figure 14: $FWHM^2$ vs peaking time from pulser data.

Cobalt-60 as a calibration source, the energy of the pulser was estimated for each peaking time. Its calibrated energy should be independent of the peaking time used, but instead a rise in calibrated energy was observed. This suggests the data acquisition set up needs to be better understood first. If the FWHM data is within a factor of around 2 of precise measurements though, it suggests an inconsistency with the results in Fig 12. The minimum FWHM is $\sim 600eV$ in contrast to $\sim 2000eV$, and the optimal peaking time is $\sim 5~\mu S$ vs .25 μS. In addition to improving data acquisition of both methods, calibration of the first method should be double checked.

5 Conclusion

The optimal peaking time of a trapezoidal filter on the CoGeNT detector was found to be between .1 and 1 μS. However, several additional checks should be done before the results can be reported with confidence. The electronic noise power spectrum contains many frequency spikes which need to be understood and eliminated. Once accomplished, this may lead to useful deconstruction of the noise into its parallel, series and 1/f components. For now, uncertainty in the 1/f noise and assumptions on the form of the parallel noise plague the results. In addition, the power spectrum calibration method and value needs to be double checked as it currently predicts $\sim 3-4\times$ the FWHM contribution of electronic noise compared to actual energy spectra measurements. Full

verification of results should not be declared until both the software analysis of raw noise and the direct FWHM measurements of pulser input are in agreement.

References

[1] R. Henning et al. The majorana demonstrator: An r&d project towards a tonne-scale germanium neutrinoless double-beta decay search.

[2] *Radiation Detection and Measurement.* John Wiley and Sons, 1999.

[3] M. Leber. *Monte Carlo Calculations of the Intrinsic Detector Backgrounds for the Karlsruhe Tritium Neutrino Experiment.* PhD thesis, UW, 2010.

[4] *Semiconductor Detector Systems.* Oxford Science Publications, 2005.

[5] H. S. W. C. Tseung. *Simulation of the Sudbury Neutrino Observatory Neutral Current Detectors.* PhD thesis, Oxford, 2008.

[6] M. Marino. *Dark Matter Physics with P-type Point-contact Germanium Detectors.* PhD thesis, UW, 2010.